Tauziède-Espariat *et al.*
Acta Neuropathologica Communications (2025) 13:131
https://doi.org/10.1186/s40478-025-02044-6

Acta Neuropathologica Communications

RESEARCH

Open Access

ATRX loss in adult gliomas lacking H3 alterations or IDH mutations, an exceptional situation for exceptional diagnoses: the experience of Sainte-Anne hospital

Arnault Tauziède-Espariat[1,2,3*], Alexandre Roux[2,3,4], Joseph Benzakoun[2,3,5], Paul Kauv[6], Sanaa Tazi[7], Alice Métais[1,2,3], Abigail K. Suwala[8,9,10], ·Felix Hinz[8,9], ·Lauren Hasty[1], Mathilde Filser[11], Julien Masliah-Planchon[11], Raphaël Saffroy[12], Margot Bucau[13], Johan Pallud[2,3,4] and Pascale Varlet[1,2,3]

Abstract

ATRX immunostaining constitutes a routinely used biomarker for the practice of neuropathology. The loss of ATRX expression correlating with *ATRX* gene alterations is implicated in a wide variety of pediatric and adult gliomas, and has been indexed as a desirable or essential diagnostic criterion for four tumor types featured in the latest world health organization classification of central nervous system Tumors. In adult-type diffuse glioma, the loss of ATRX expression is a hallmark of astrocytoma, IDH-mutant. Recently, novel tumor types and alterations have been referenced in the literature. These include the high-grade astrocytoma with piloid features (HGAP), for which no consistent clinicopathological features have been defined, and the presence of other alterations in the Krebs cycle genes (variants of the *Fumarate hydratase* -FH- gene) found in gliomas resembling astrocytomas, IDH-mutant. Because of this rapidly evolving classification and histomolecular landscape, we retrospectively analyzed adult gliomas diagnosed over a four consecutive year period to identify supratentorial gliomas, lacking H3 alterations or IDH mutations and harboring a loss of ATRX expression, in order to update their diagnoses in terms of histopathology, genetics and epigenetics. Four specimens (from 620 adult gliomas, 0.7%) were reclassified at the end of the molecular workup, as: 1/ one HGAP, 2/ one malignant transformation with a primitive neuronal component of an astrocytoma, IDH-mutant which lost the *IDH2* mutation at recurrence, 3/ a glioma, *FH*-mutant for which the histopathological and epigenetic features were similar to an astrocytoma, IDH-mutant, and 4/ a glioblastoma, IDH-wildtype. To conclude, these exceptional cases extend the spectrum of ATRX loss in gliomas, beyond the astrocytoma, IDH-mutant and the diffuse hemispheric glioma, H3 G34-mutant.

Keywords ATRX, Diffuse glioma, FH, HGAP

*Correspondence:
Arnault Tauziède-Espariat
a.tauziede-espariat@ghu-paris.fr
Full list of author information is available at the end of the article

Introduction

The *ATRX* (α-thalassemia/x-linked intellectual disability syndrome) gene, located on chromosome Xq21.1, is a tumor gene suppressor implicated in the incorporation of the histone variant H3.3 on pericentric heterochromatin and on telomeres, as well as in several transcription factor binding sites. Mutations of this gene have been encountered in several glial tumor types. These alterations induce the generation of a truncated protein which results in a loss of nuclear immunoreactivity in tumor cells [1]. Consequently, neuropathologists routinely use ATRX immunohistochemistry as ATRX expression/*ATRX* alterations constitute an essential or a desirable criterion for three tumor types in the latest World Health Organization (WHO) Classification of Central Nervous System (CNS) Tumors: astrocytoma, IDH-mutant [1–3], diffuse hemispheric glioma, H3 G34-mutant [2], and high-grade astrocytoma with piloid features (HGAP) [4, 5]. Moreover, the loss of ATRX expression has also been identified as a potential diagnostic tool for other pediatric and adult tumor types recently described: the glioneuronal tumor with ATRX alteration, kinase fusion and anaplastic features [6], diffuse pediatric-type high-grade glioma, H3- and IDH-wildtype (WT), RTK2B subtype [7], and diffuse midline glioma subtype, H3K27/MAPKinase co-altered [8]. To complexify this histomolecular landscape, two recent observations have evidenced that rare diffuse gliomas resembling astrocytomas, IDH-mutant may harbor mutations of another gene implicated in the Krebs cycle, the *Fumarate Hydratase* (*FH*) gene, which induces a loss of expression for the FH protein [9, 10]. In this rapidly evolving field, we report here four observations of adult supratentorial diffuse gliomas, lacking H3 alterations or IDH mutations and harboring a loss of ATRX expression and representing diagnostic pitfalls or challenges.

Materials and methods

Sample selection

From a cohort of 620 adult gliomas (comprised of 152 gliomas, IDH-mutant (93 astrocytomas, IDH-mutant and 59 oligodendrogliomas, IDH-mutant and 1p/19q codeleted), and 468 glioblastomas, IDH-WT) diagnosed between 01/01/2017 and 31/12/2020, we extracted all supratentorial gliomas, lacking H3 alterations or IDH mutations presenting a loss of ATRX expression from the detailed reports and re-actualised their diagnoses.

Histopathological review and immunohistochemistry

The central pathology review was performed by two neuropathologists (ATE, and PV). A representative paraffin block was selected for each sample. 3-µm-thick slides of formalin-fixed, paraffin-embedded (FFPE) tissues were used for immunostaining. The following primary antibodies were used: OLIG2 (1:500, clone EP112, Roche Diagnostics GmbH, Mannheim, Deutschland), neurofilament protein (NF) (1:100, clone 2F11, Dako, Glostrup, Denmark), Synaptophysin (1:150, clone DAK-SYNAP, Dako, Glostrup, Denmark), H3K27me3 (1:2500, polyclonal, Diagenode, Liege, Belgium), EZHIP (1:75, polyclonal, Sigma-Aldrich, Bromma, Sweden), H3K27M (1:5000, clone EPR18340, Abcam, Cambridge, United Kingdom), H3G34R (1:1000, clone EPR23519, Abcam, Cambridge, United Kingdom), BRAFV600E (1:100; clone VE1, Spring Biosciences, Pleasanton, United States of America), p53 (1:5000, clone DO-1, Santa Cruz Biotechnology, Dallas, United States of America), FGFR3 (1:150, clone B-9, Santa Cruz Biotechnology, Dallas, United States of America), RB1 (1:200, clone G3-245, Becton Dickinson, Rungis, France), MSH2 (pre-diluted, clone FE11, Dako, Glostrup, Denmark), MSH6 (pre-diluted, clone 44, Dako, Glostrup, Denmark), MLH1 (pre-diluted, clone E505, Dako, Glostrup, Denmark), PMS2 (pre-diluted, clone EPR3947, Dako, Glostrup, Denmark), and Fumarate Hydratase (FH) (1:500, clone J-13, Santa Cruz Biotechnology, Dallas, United States of America). External positive and negative controls were used for all antibodies.

Fluorescent in situ *hybridization (FISH)*

Fluorescence in situ hybridization (FISH) analyses were performed on representative paraffin-embedded tumor sections. The following probe was used: *MYCN* (Zytovision, Zyto*Light* SPEC MYCN/2q11 Dual Color Probe). FISH studies were realized as previously described [11]. Signals were scored in at least 100 non-overlapping interphase nuclei. Specimens were considered amplified if ≥ 8 signals were detected in more than 10% of nuclei [12].

RNA sequencing data

RNA was extracted from two 8-µm-thick formalin-fixed paraffin-embedded (FFPE) material sections using the high Pure FFPE RNA Isolation Kit (Roche Diagnostics, Boulogne-Billancourt, France) in accordance with the manufacturer's instruction. RNA concentrations were measured on a Qubit 4 Fluorometer (Thermo Fisher Scientific, USA) with the Invitrogen Qubit RNA BR Kit (Thermo Fisher Scientific). The percentage of RNA fragments > 200nt (fragment distribution value; DV200) was evaluated by capillary electrophoresis (Agilent 2100 Bioanalyzer). A DV200 > 30% was required to process the next steps in the analysis. Next-generation sequencing (NGS)-based RNA sequencing was performed using the Illumina TruSight RNA Fusion Panel on a NextSeq550 instrument according to the manufacturer's instructions (Illumina, San Diego, CA, USA). This targeted

RNA sequencing panel covers 507 fusion-associated genes, to assess the most known cancer-related fusions. The TruSight RNA Fusion Panel gene list is available at https://www.illumina.com/content/dam/illumina-marketing/documents/products/gene_lists/gene_list_trusight_rna_fusion_panel.xlsx. A total of 7690 exonic regions were targeted with 21,283 probes. Libraries were prepared according to the Illumina instructions for the TruSight RNA Fusion Panel kit. STAR_v2.6.1a or Bowtie software was used to produce aligned reads in relation to the Homo sapiens reference genome (UCSC hg19)[13]. Manta v1.4.0, TopHat2 and Arriba tools were used for fusion calling[14].

Next-generation sequencing (NGS)

Next-generation sequencing (NGS) was also performed according to the Illumina NextSeq 500 protocol (Illumina, San Digeo, CA, USA), which allowed us to detect mutations for *BRAF, FGFR1, PTPN11, KRAS, NRAS* and *HRAS*. We employed a custom NGS panel known as DRAGON (Detection of Relevant Alterations in Genes involved in Oncogenetics by NGS), commercially available as SureSelect CD Curie CGP by Agilent. This panel encompasses 571 oncology-related genes, serving diagnostic, prognostic, therapeutic, and predisposition purposes. It covers nucleotide sequences (variants) and copy number alterations (deletions and focal amplifications). Library preparation involved using 50 ng of DNA extracted from frozen tumors with the Agilent SureSelect XT-HS preparation kit, following the manufacturer's protocol. In addition to the 571 genes, the panel incorporates genome-wide probes, offering a copy number profile with an average resolution of one probe every 200 Kb. This allows for a comprehensive copy number profile across all chromosomes. Variant calling was performed using Varscan2 (v2.4.3), while copy number profiles for each tumor were estimated using a combination of in-house R scripts and the facets package (v0.6.0). We used a sex-specific unmatched-germline control sequenced with the same panel for normalization.

DNA methylation profiling and copy number variant calculation

Tissue samples (FFPE), for which 500 ng of DNA was extracted, were analyzed. DNA was extracted using the QIAamp® DNA Tissue kit or QIAamp® DNA FFPE Tissue Kit (Qiagen, Hilden, Germany) for FFPE samples. DNA from FFPE samples was restored using the Infinium HD FFPE Restore Kit (Illumina, San Diego, California, USA). Bisulfite conversion was performed using the Zymo EZ DNA methylation Kit (Zymo Research, Irvine, California, USA). Standard quality controls confirmed DNA quality/quantity and bisulfite conversion. DNA was then processed using either Illumina Infinium Methylation EPIC or HumanMethylation450 BeadChip (Illumina, San Diego, California, USA) arrays according to the manufacturer's instructions. The iScan control software was used to generate raw data files in.idat format, analyzed using GenomeStudio software version v2011 and checked for quality measures according to the manufacturer's instructions. To complement these raw data and as a reference, 406 samples were added from Capper et al. containing different methylation classes corresponding to the DKFZ v11b4 classification (updated with brain classifier version 12.8). Affiliation predictions for CNS tumor classes were obtained from a DNA methylation-based classification of CNS tumors from DKFZ (Deutsches Krebsforschungszentrum—German Cancer Research Center) based on a random forest algorithm available on the web platform www.molecularneuropathology.org. Version v12.8 of the algorithm and the v2.0 of the Bethesda classifier were used for the present study. The output of these classifiers is a score (calibrated score) indicating the classification to the reference CNS tumor class in the algorithm. Summary copy number plots were generated using an in-house R-script (https:// github.com/ dstic hel/ CNsum maryp lots).

Clinical and imaging data

The following clinical data were acquired for each patient using a dedicated datasheet: sex, age at imaging diagnosis, age at histopathological diagnosis, past medical history, clinical presentation, tumor resection state, radiotherapy, chemotherapy, event-free survival (EFS) and overall survival (OS). All four cases underwent central imaging review by experienced radiologists (PK and JB). The following features were evaluated: tumor location, size, diffusion signal and apparent coefficient diffusion (ADC), contrast enhancement, necrosis, edema, and perfusion parameters.

Case histories

Case 1

A 27-year-old man was referred for headaches. Magnetic resonance imaging (MRI) revealed an infiltrating capsulo-thalamic lesion with FLAIR hyperintensity (Fig. 1A and B). The lesion was non-homogeneously contrast-enhanced (Fig. 1C). A biopsy was performed. Histopathologically, the sample concerned a diffuse glial proliferation composed of astrocytic and multinucleated cells with numerous mitoses (Fig. 1D). There was no necrosis or microvascular proliferation in the biopsy sample. There were no Rosenthal fibres, ganglionic cells, eosinophilic granular bodies, inflammatory infiltrates, or xanthomatous changes. The neurofilament staining confirmed the diffuse growth pattern of the tumor. The

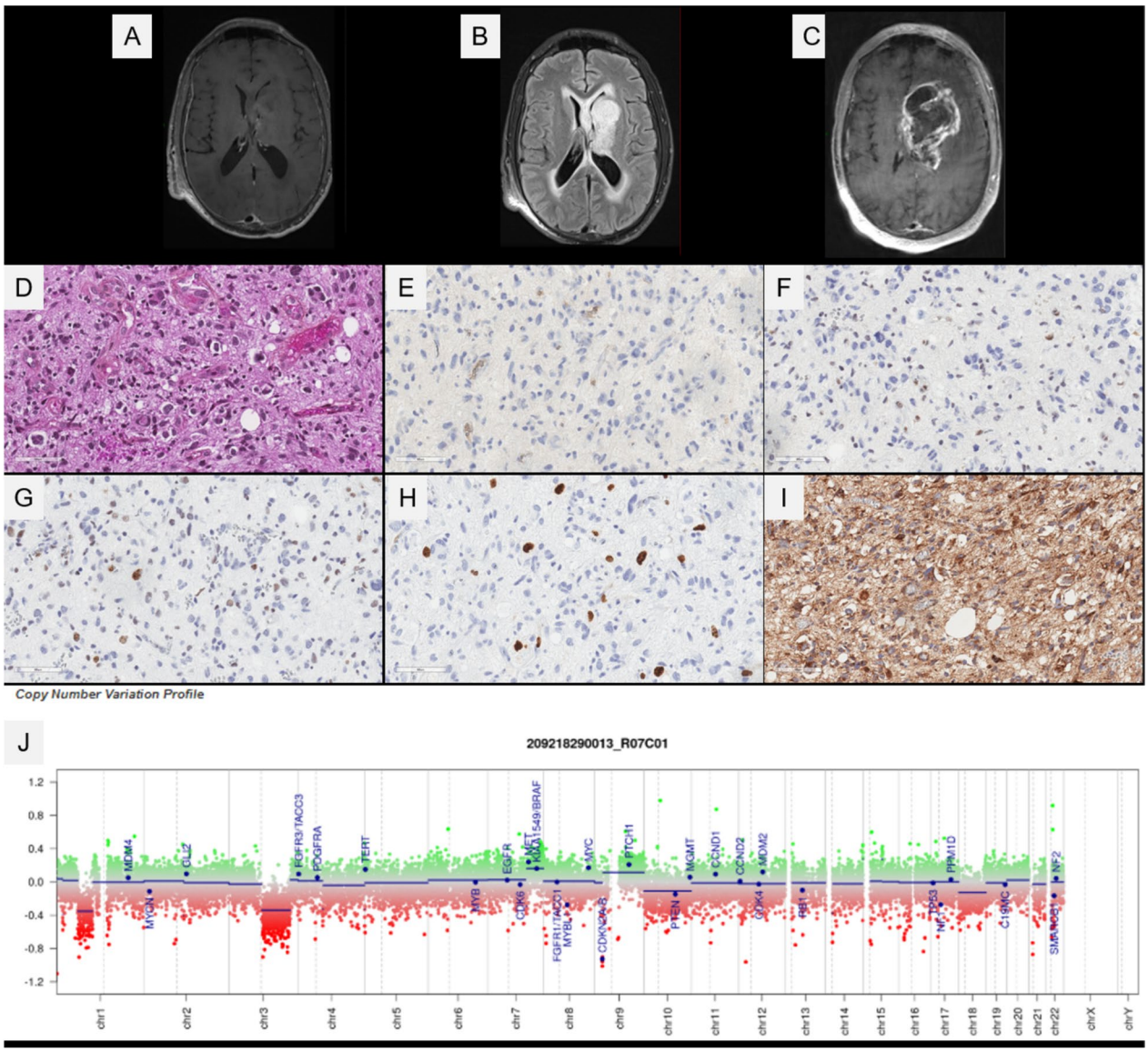

Fig. 1 Imaging, histopathological and molecular features of the case #4. (**A**) A capsulo-thalamic infiltrating lesion without initial enhancement after gadolinium injection but FLAIR hyperintensity (**B**). This tumor was non-homogeneously enhanced after gadolinium injection during the following MRI of the follow-up (**C**). (**D**) A diffuse glial proliferation composed of astrocytic and multinucleated cells with numerous mitoses (HPS, magnification × 400). (**E**) No immunoexpression for IDH1R132H (magnification × 400). (**F**) A loss of ATRX expression (magnification × 400). (**G**) No overexpression of p53 (magnification × 400). (**H**) Elevated proliferative index (MIB1, magnification × 400). (**I**) A preserved expression of FH (magnification × 400). (**J**) Copy number variation analysis showing a homozygous deletion of the *CDKN2A* gene. Black scale bars represent 60 µm. HPS: Hematoxylin Phloxin Saffron

tumor cells diffusely expressed OLIG2 and H3K27me3 was maintained. There was no immunoexpression for IDH1R132H (Fig. 1E), H3K27M, EZHIP, or H3G34R. There was a loss of ATRX expression and no overexpression of p53 (Fig. 1F and G). The proliferative index was high (Fig. 1H). The expression of MMR proteins and FH were preserved (Fig. 1I). A NGS analysis evidenced a mutation of the *ATRX* and *NF1* genes and a homozygous deletion of *CDKN2A* (Fig. 1J). The neurooncologist communicated information concerning a context of type 1 neurofibromatosis. DNA-methylation profiling classed the tumor as HGAP (calibrated scores of 0.99, using the DKFZ classifier, v12.8, and Bethesda classifier v2.0). The patient received radiation therapy and chemotherapy (Temozolomide), and died 24 months after the initial diagnosis from tumor progression.

Case 2

A 29-year-old man was diagnosed two years ago with a right frontal diffuse astrocytoma, IDH-mutant (grade 2) with *IDH2* R172S, *ATRX* and *TP53* mutations (Fig. 2A–D). The histopathology was classic for a diffuse astrocytoma, IDH-mutant (Fig. 2E–G). The tumor was initially subtotally resected and radiological and clinical surveillance was carried out. Two years after the initial diagnosis, an MRI evidenced an in situ recurrence revealed by confusion and hemiparesis (Fig. 2H–K). A novel surgery was performed. Histopathologically, the tumor was different than the first sample, composed of solid nodules showing immature cells with numerous mitoses, extensive necrosis, and microvascular proliferation (Fig. 2L). The tumor cells focally expressed OLIG2 and diffusely expressed synaptophysin (Fig. 2M and N). There was an overexpression of p53, a loss of ATRX expression (Fig. 2O and P), and a significantly reduced expression for RB1 (not shown). IDH1R132H was negative. The expression of MMR proteins and FH were preserved. The NGS analysis found the same *TP53* and *ATRX* mutations as the first surgery, but there were no *IDH1/2* mutations the second time. The FISH analysis evidenced a *MYCN* high-level amplification (Fig. 2Q) and no *CDKN2A/B* deletion. DNA-methylation profiling analysis determined it was an astrocytoma, IDH-mutant, higher grade (calibrated score of 0.51, using DKFZ classifier, v12.8, and calibrated score of 0.99, using Bethesda classifier, v2.0). A t-sne analysis, which included a primitive neuronal component, IDH-mutant astrocytomas was performed, showing that the case clustered within this methylation class (Supplementary Fig. 1). Treatment by radiation therapy and chemotherapy (Temozolomide) was initialized, but the patient died five months after the second surgery.

Case 3

A 74-year-old man experienced symptoms of raised intracranial pressure. An MRI revealed a lesion in the third ventricle showing heterogeneous enhancement after the injection of gadolinium (Fig. 3A–C). A tumor biopsy was performed. Histopathologically, the biopsy revealed a diffuse glioma with an astrocytic proliferation, showing several mitoses and a microvascular proliferation (Fig. 3D). There was no necrosis. The neurofilament staining confirmed the infiltrating tumor growth. Tumor cells expressed OLIG2 and H3K27me3. There was a loss of ATRX expression (Fig. 3E) without immunopositivity for IDH1R132H. The expression of MMR proteins was preserved. The NGS analysis confirmed the presence of an *ATRX* mutation associated with a *PIK3CA* variant, but without *IDH1/2* and *TP53* mutations. The DNA-methylation profiling analysis concluded it was a diffuse glioma, IDH-mutant (calibrated score of 0.65 using DKFZ classifier v12.8, and 0.98 Bethesda classifier v2.0), and subtype astrocytoma, IDH-mutant, low grade (calibrated score of 0.48 Bethesda classifier v2.0). Retrospectively, an FH immunostaining was performed and showed a complete loss of expression in tumor cells, and a complementary sequencing analysis revealed the presence of an *FH* mutation (Fig. 3F). Because of an initial diagnosis of glioblastoma, the patient received chemotherapy (Temozolomide) and radiation therapy. Currently, the patient is alive with a stable disease 56 months after the initial diagnosis.

Case 4

A 38-year-old woman experienced headaches, and paresthesia on the right side of her body. MRI revealed a left temporo-parietal lesion of the third ventricle with infiltration of the *corpus callosum* heterogeneously enhanced after injection of gadolinium (Fig. 4A–E). A tumor biopsy was performed. Histopathologically, the biopsy concerned a diffuse glioma with an astrocytic proliferation, showing several mitoses and a microvascular proliferation (Fig. 4F). There was no necrosis. Multinucleated cells and microcalcifications were observed. The neurofilament staining confirmed the infiltrating tumor growth. Tumor cells expressed OLIG2 and H3K27me3. There was no IDH1R132H, BRAFV600E or FGFR3 immunopositivity but a loss of ATRX expression, a p53 overexpression and a high proliferative index (Fig. 4G–J). The expression of MMR proteins and FH were preserved (Fig. 4K). NGS analysis confirmed the presence of an *ATRX* mutation associated with a *TP53* variant and a homozygous deletion of *CDKN2A*, without *IDH1/2* mutations. RNA-sequencing analysis failed to reveal any fusion. The DNA-methylation profiling analysis concluded with a glioblastoma, mesenchymal type (calibrated score of 0.45, using DKFZ classifier v12.8, and calibrated score of 0.80 using Bethesda classifier v2.0). The copy number variation analysis showed a gain of chromosome 7, without the loss of chromosome 10, and amplifications of the *MDM2* and *CDK4* genes without *EGFR* amplification (Fig. 4L). The final diagnosis was a glioblastoma, IDH-WT. Treatment by radiation therapy and chemotherapy (Temozlomide) was initialized, but the patient died three weeks after the biopsy.

Discussion

ATRX immunostaining is now largely included in the routine diagnostic panel of neuropathologists. The loss of ATRX expression currently constitutes a hallmark of several pediatric and adult tumor types. In adult-type glioma, the main diagnosis is the astrocytoma, IDH-mutant, which presents a loss of expression in more than 90% of supratentorial specimens [15]. When ATRX expression is preserved,

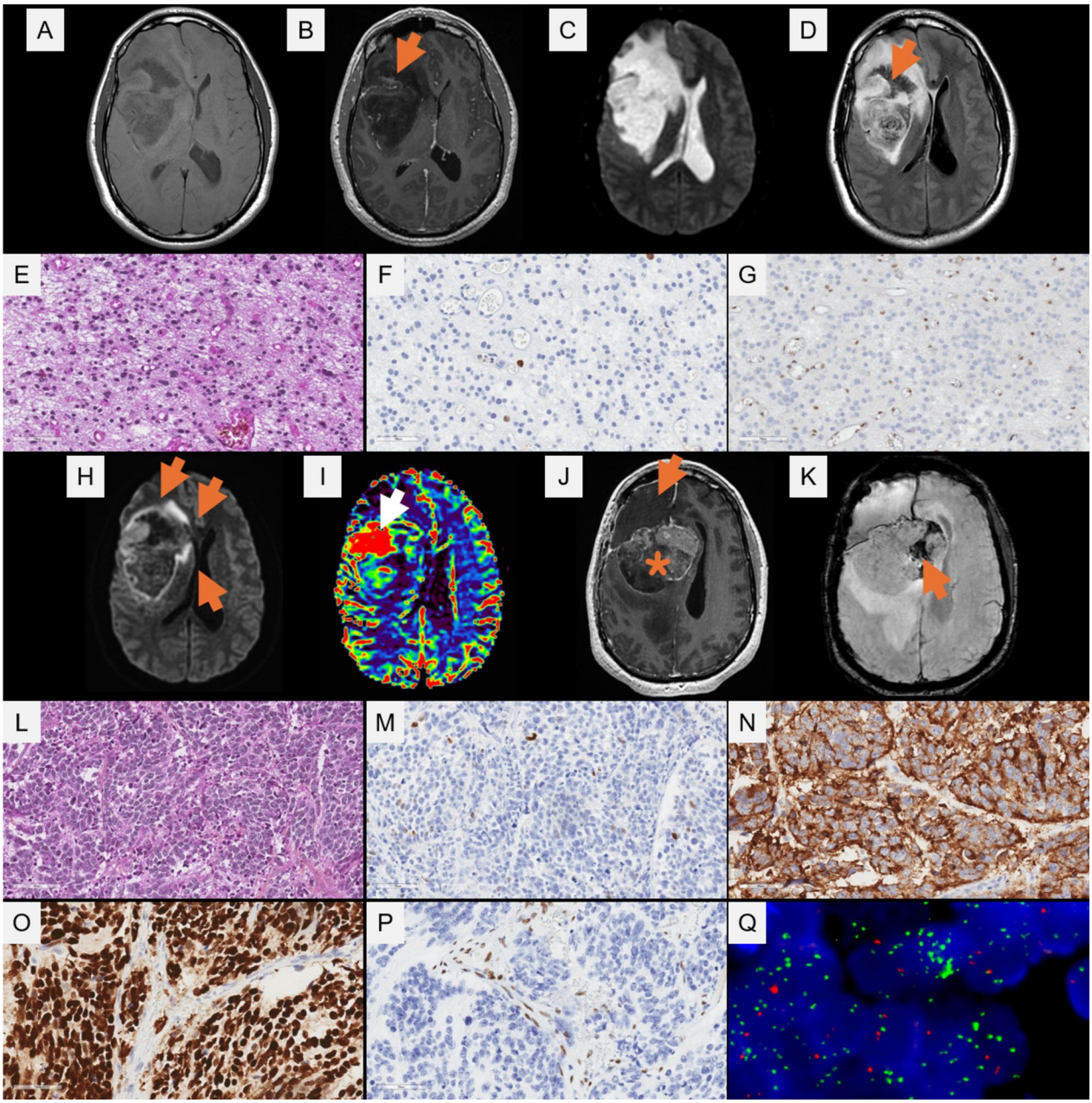

Fig. 2 Imaging, histopathological and molecular features of case #2. Axial T1 sequence before (**A**) and after contrast injection (**B**) displayed a large right hemispheric lesion with slight subcortical enhancement (arrow in **B**), associated with mass effect and brain herniation under the falx cerebri. T2-weighted sequence (**C**) and T2-FLAIR sequence (**D**) displayed a hyper-intense liquid central contingent (arrow in **D**) in T2 and signal suppression in FLAIR. (**E**) A diffuse astrocytoma (HPS, magnification × 400) with a low proliferative index (**F**, magnification × 400), and loss of ATRX expression (**G**, magnification × 400). Two years after the initial surgery, diffusion-weighted imaging (**H**) displayed a rim with diffusion restriction (arrows), suggesting hypercellularity. Relative Cerebral Volume (rCBV) map (**I**) computed from Perfusion-Weighted Imaging, displayed a hyperperfused area in the frontal region (rCBV = 5), suggesting the presence of an intermediate or high grade component. Axial T1 sequence after contrast injection (**J**) displayed a large mass (star) posterior to the postoperative cavity (arrow) with partial enhancement suggesting intratumoral necrosis. Susceptibility imaging (**K**) displayed hemorrhagic areas (arrow). The recurrent tumor was histopathologically different, composed of solid nodules showing immature cells with numerous mitoses (**L**). **(M)** Focal expression of OLIG2 (magnification × 400), and diffuse immunoreactivity for synaptophysin (**N**, magnification × 400). (**O**) Overexpression of p53 (magnification × 400). **P** loss of ATRX expression (magnification × 400). **Q** High-level amplification of *MYCN* locus (magnification × 400, *MYCN* locus: green signals, centromere of chromosome 2: orange signals). Black scale bars represent 60 µm. HPS: Hematoxylin Phloxin Saffron

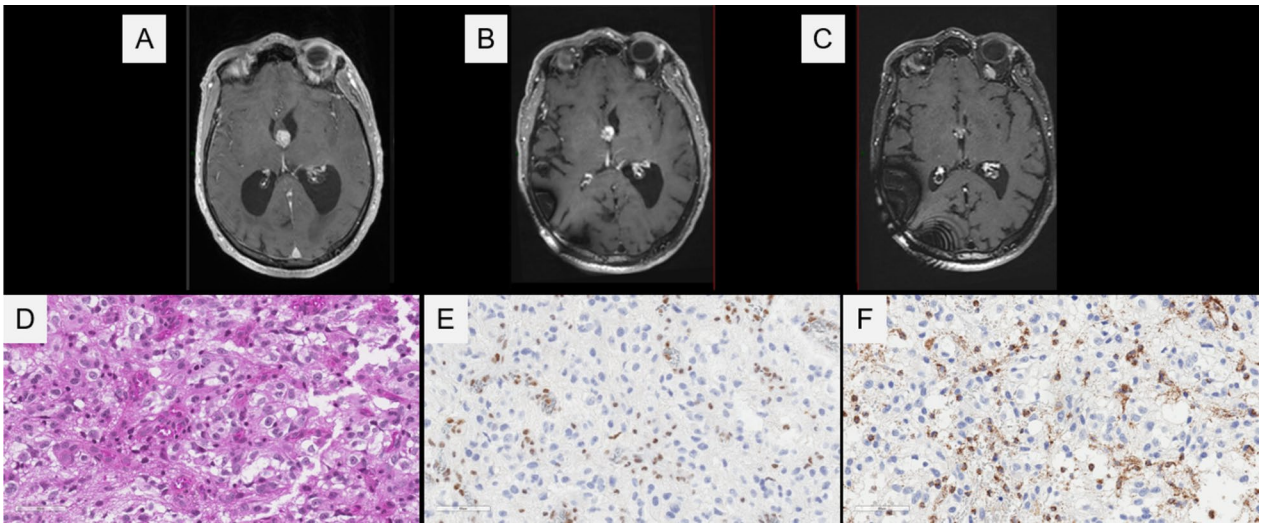

Fig. 3 Imaging, histopathological and molecular features of case #3. A lesion in the third ventricle with heterogeneous enhancement after the injection of gadolinium (**A-C**). (**D**) A diffuse glioma with an astrocytic proliferation, showing several mitoses and a microvascular proliferation (HPS, magnification × 400). (**E**) A loss of expression of ATRX (magnification × 400). (**F**) The FH immunostaining showed a complete loss of expression in tumor cells, and a preserved expression of residual glial cells in the parenchyma (magnification × 400). Black scale bars represent 60 µm. HPS: Hematoxylin Phloxin Saffron

the presence of *TP53* alterations can be supportive of the presence of an astrocytoma rather than an oligodendroglioma [2, 16]. Regarding the recent literature, neuropathologists have to be mindful of two pitfalls illustrated in this study. Firstly, the *IDH1/2* driver mutation may disappear at recurrence: it may be observed in malignant [17] or sarcomatous transformations [18], or in the case of a neuronal primitive component differentiation in an astrocytoma, IDH-mutant [19]. Interestingly, DNA-methylation analyses still classified these recurrent poorly differentiated tumors as "gliomas, IDH-mutant" [18, 19]. Yamaguchi J. et al. reported an astrocytoma, IDH-mutant which transformed into a malignant form with a primitive neuronal component [19]. This component was not mutated for the *IDH1/2* genes and was classified as an astrocytoma, IDH-mutant; High Grade with a low score of 0.61 [19]. Herein, we show that the DNA-methylation profile of this recurrence clustered with IDH-mutant astrocytomas having a primitive neuronal component, which constitute a distinct methylation class, associated with a poorer prognosis than classical astrocytomas, IDH-mutant (grades 2 and 3), and recurrent alterations (*MYCN* amplification and *RB1* deletion) [20]. However, in this cohort, only primary tumors were included and using immunohistochemistry, both classical astrocytic and primitive neuronal component astrocytomas expressed the IDH1R132H mutation [20]. Our observation and that of Yamaguchi J. et al. [19] may represent an example of a clonal selection presenting as the primary tumor *ATRX* and *TP53* mutations, but with additional molecular features (*MYCN* amplification). This situation illustrates the difficulty of suggesting this diagnosis if the anteriority of astrocytoma, IDH-mutant is not known. Or in case a of late de novo diagnosis. In this context, differentiating this diagnosis from a glioblastoma, IDH-mutant with a primitive neuronal component may be challenging and long clinical history can help. However, this tumor type does not present a loss of ATRX expression/*ATRX* alterations [21, 22], and a distinct methylation class for glioblastoma, with neuronal primitive component exists. Secondly, in the "IDH" area, neuropathologists should be aware of another recently described pitfall. Indeed, the current case #3 represents the third example of an astrocytoma, IDH-mutant without an *IDH1/2* variant but with an *FH* alteration [9]. FH is part of the citrate cycle, like IDH1/2, and it has been shown that FH loss, via the accumulation of FH substrate fumarate, activates a series of oncogenic cascades whose contribution to transformation is still under investigation [23]. FH is routinely used in pathology, for uterine leiomyomas and renal cell carcinomas [24, 25]. Consequently, FH immunostaining may be useful when faced with a DNA-methylation profile or the histopathology (including loss of ATRX expression) of an astrocytoma, IDH-mutant without any *IDH1/2* mutations identified. The frequency of *FH* alterations in the glioma, IDH-mutant landscape needs to be determined in further cohorts. Thus, FH immunostaining may constitute an excellent diagnostic screening tool. The current work has evidenced an *FH* alteration in only one glioma over a period of four consecutive years, during which 153 "gliomas, IDH-mutant" were diagnosed. However, this proportion may be biased because other gliomas,

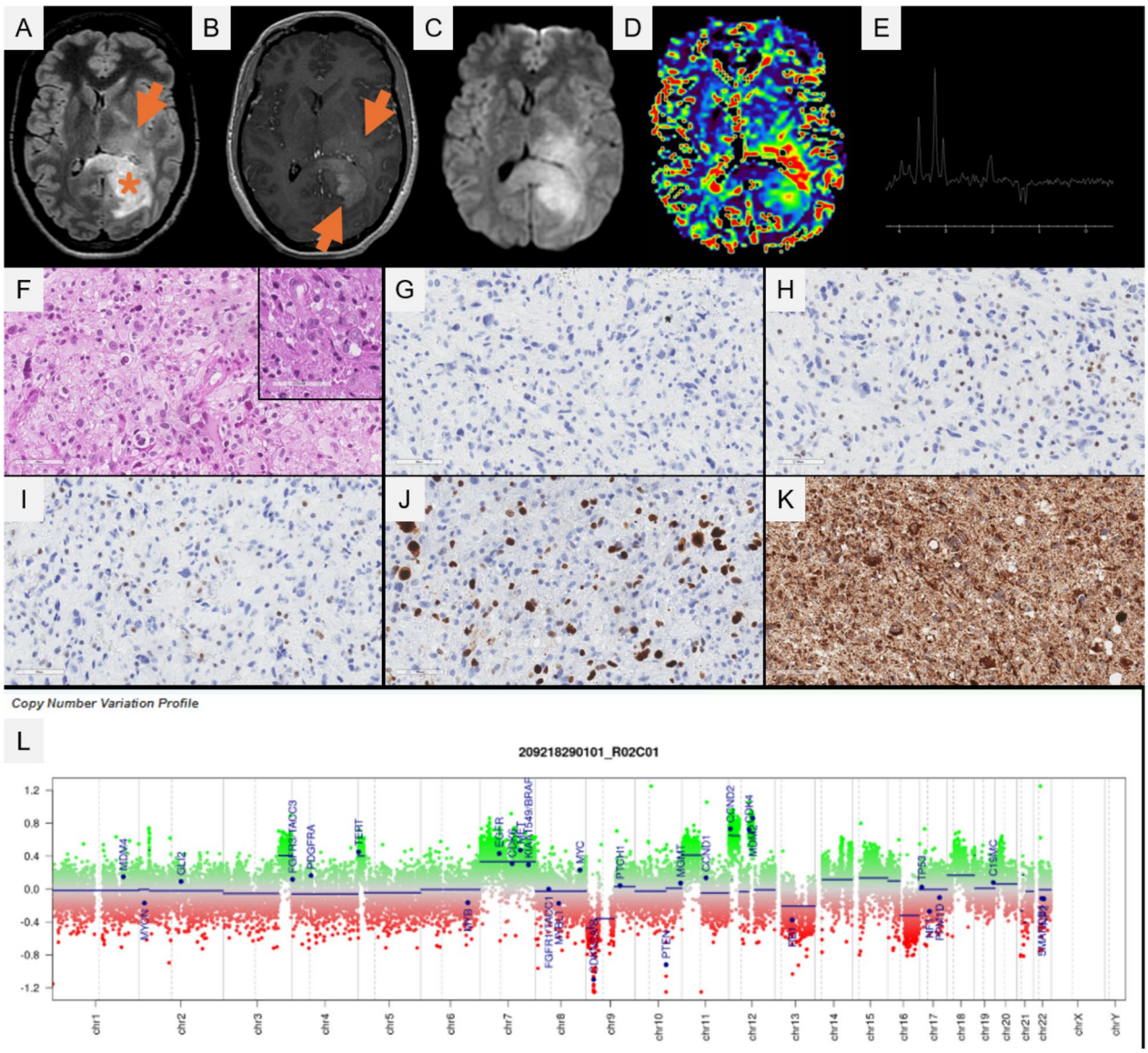

Fig. 4 Imaging, histopathological and molecular features of case #4. Axial T2-FLAIR sequence (**A**) displayed a mass centered on the left part of the corpus callosum splenium (star in A), associated with a left hemispheric infiltration with high FLAIR intensity (arrow in A). After contrast injection, axial T1 sequence (**B**) displayed a diffuse, non-necrotic enhancement on the mass bulk (arrows in B). Diffusion Weighted Imaging (**C**) displayed high intensity areas inside the mass, suggesting tumoral hypercellularity. Relative Cerebral Volume (rCBV) map (**D**) computed from Perfusion-Weighted Imaging, displayed a hyper-perfused area in the periventricular region (rCBV = 2.5), suggesting the presence of an intermediate or high grade contingent. Spectroscopic analysis with long Echo Time (TE = 144 ms) (**E**) displayed a myoinositol peak suggestive of a glial origin, an increase of choline, and a decrease of N-Acetyl-Aspartate, suggestive of hypercellularity and lactate peaks, suggestive of anaerobic metabolism. (**F**) A diffuse glioma with an astrocytic proliferation, showing atypicalities, multinucleated cells and a microvascular proliferation (HPS, magnification × 400, insert HPS magnification × 400). (**G**) No immunopositivity for IDH1R132H (magnification × 400). (**H**) Loss of expression of ATRX (magnification × 400). (**I**) No overexpression of p53 (magnification × 400). (**J**) Eleavted proliferative index (MIB1, magnification × 400). (**K**) Preserved expression of FH (magnification × 400). (**L**) The copy number variation analysis showed a gain of chromosome 7, without a loss of chromosome 10, and amplifications of the *MDM2* and *CDK4* genes without *EGFR* amplification. Black scale bars represent 60 µm. HPS: Hematoxylin Phloxin Saffron

FH-mutant without the loss of ATRX expression (but perhaps only an overexpression of p53) have potentially been misdiagnosed. Over the past few years, neuropathologists have become familiar with HGAP and it has been included in the latest WHO Classification of CNS Tumors [3]. However, this diagnosis remains a challenge due to inconsistent clinical, histopathological and genetic features. Indeed, although the loss of ATRX expression may

prompt neuropathologists to suggest this tumor type, this immunophenotype is not consistently observed (reported in 58.5% of specimens in a series of 111 HGAP (26)). Moreover, while the posterior fossa represents a common location, the literature and the current case #4 illustrate that supratentorial examples are possible [26]. Furthermore, although this tumor type was included in the chapter of circumscribed astrocytic gliomas, HGAP can frequently be partially infiltrating, making this diagnosis a potential pitfall for other diffuse gliomas encountered in adults [4, 27, 28]. Therefore, the sole tool for the diagnosis of HGAP still remains DNA-methylation profiling. Finally, the loss of ATRX expression seems to be very rare in glioblastomas, IDH-mutant, representing only 4.5% of specimens from a previous series [29], but this frequency was estimated before the era of DNA-methylation profiling, and has to re-evaluated in further cohorts with actualized diagnoses.

To conclude, in an adult subpopulation, the loss of ATRX expression should prompt neuropathologists to carry out genetic and epigenetic investigations before establishing a diagnosis of glioblastoma, IDH-WT.

Abbreviations

GBM PNC	Glioblastoma with neuronal primitive component
IDH PNC	Astrocytoma, IDH-mutant, with neuronal primitive component
MB_SHH_IDH	Medulloblastoma, SHH-activated, IDH-mutant
PMMDIA	Constitutional mismatch repair deficient astrocytoma, IDH-mutant

Supplementary Information

The online version contains supplementary material available at https://doi.org/10.1186/s40478-025-02044-6.

Additional file1 (TIF 14505 KB)

Acknowledgements
We would like to thank the laboratory technicians at GHU Paris Neuro Sainte-Anne for their assistance.

Author contributions
ATE, AR, JB, PK, ST, and JP compiled the MRI and clinical records; ATE, AM, MB, and PV conducted the neuropathological examinations; ATE, AKS, FH, MF, JMP, and RS conducted the molecular studies; PV, LH and ATE drafted the manuscript; all authors reviewed the manuscript.

Funding
The authors have received no external funding for this study.

Data availability
No datasets were generated or analysed during the current study.

Declarations

Ethics approval and consent to participate
This study was approved by GHU Paris Psychiatry and Neurosciences, Sainte-Anne Hospital's local ethic committee.

Consent for publication
The patient signed informed consent forms before treatment was started.

Competing interests
The authors declare that they have no conflicts of interest directly related to the topic of this article.

Author details
[1]Department of Neuropathology, GHU Paris-Psychiatrie et Neurosciences, Sainte-Anne Hospital, Paris, France. [2]Institut de Psychiatrie et Neurosciences de Paris (IPNP), UMR S1266, INSERM, IMA-BRAIN, Paris, France. [3]Université de Paris, Paris, France. [4]Department of Neurosurgery, GHU Paris-Psychiatrie et Neurosciences, Sainte-Anne Hospital, 75014 Paris, France. [5]Neuroradiology Department, GHU Paris-Psychiatrie et Neurosciences, Sainte-Anne Hospital, Paris, France. [6]Neuroradiology Department, Henri Mondor Hospital, Créteil, France. [7]Neurosurgery Department, Henri Mondor Hospital, Créteil, France. [8]Department of Neuropathology, Institute of Pathology, Heidelberg University Hospital, Heidelberg, Germany. [9]Clinical Cooperation Unit Neuropathology, German Cancer Research Center (DKFZ), German Consortium for Translational Cancer Research (DKTK), Heidelberg, Germany. [10]Department of Neurological Surgery, Helen Diller Research Center, University of California San Francisco, San Francisco, CA, USA. [11]Laboratory of Somatic Genetics, Institute Curie Hospital, Paris, France. [12]Department of Biochemistry and Oncogenetics, Paul Brousse Hospital, 94804 Villejuif, France. [13]Department of Pathology, Bichat Hospital, Paris, France.

Received: 7 April 2025 Accepted: 21 May 2025
Published online: 13 June 2025

References

1. Reuss DE, Sahm F, Schrimpf D, Wiestler B, Capper D, Koelsche C et al (2015) ATRX and IDH1-R132H immunohistochemistry with subsequent copy number analysis and IDH sequencing as a basis for an "integrated" diagnostic approach for adult astrocytoma, oligodendroglioma and glioblastoma. Acta Neuropathol (Berl) 129(1):133–146
2. Ebrahimi A, Skardelly M, Bonzheim I, Ott I, Mühleisen H, Eckert F et al (2016) ATRX immunostaining predicts IDH and H3F3A status in gliomas. Acta Neuropathol Commun 4(1):60
3. Louis DN, Perry A, Wesseling P, Brat DJ, Cree IA, Figarella-Branger D et al (2021) The 2021 WHO classification of tumors of the central nervous system: a summary. Neuro-Oncol 23(8):1231–1251
4. Reinhardt A, Stichel D, Schrimpf D, Sahm F, Korshunov A, Reuss DE et al (2018) Anaplastic astrocytoma with piloid features, a novel molecular class of IDH wildtype glioma with recurrent MAPK pathway, CDKN2A/B and ATRX alterations. Acta Neuropathol (Berl) 136(2):273–291
5. Bender K, Perez E, Chirica M, Onken J, Kahn J, Brenner W et al (2021) High-grade astrocytoma with piloid features (HGAP): the Charité experience with a new central nervous system tumor entity. J Neurooncol 153(1):109–120
6. Bogumil H, Sill M, Schrimpf D, Ismer B, Blume C, Rahmanzade R et al (2023) Glioneuronal tumor with ATRX alteration, kinase fusion and anaplastic features (GTAKA): a molecularly distinct brain tumor type with recurrent NTRK gene fusions. Acta Neuropathol (Berl) 145(5):667–680
7. Tauziède-Espariat A, Friker LL, Nussbaumer G, Bison B, Dangouloff-Ros V, Métais A et al (2024) Diffuse pediatric high-grade glioma of methylation-based RTK2A and RTK2B subclasses present distinct radiological and histomolecular features including Gliomatosis cerebri phenotype. Acta Neuropathol Commun 12(1):176
8. Tauziède-Espariat A, Castel D, Ajlil Y, Auffret L, Appay R, Mariet C et al (2024) Atrx loss as a promising screening tool for the identification of diffuse midline glioma subtype, H3K27/MAPKinase co-altered. Acta Neuropathol Commun 12(1):105
9. Zschernack V, Thomas C, Schaub C, Kristiansen G, Waha A, Goschzik T et al (2024) FH-mutant glioma displaying the epigenetic signature of IDH-mutant astrocytomas. J Neuropathol Exp Neurol 83(10):887–889
10. Raghunathan A, Ida CM, Westbroek EM, Gupta S, Jenkins RB, Giannini C et al (2022) Mutations of FH and IDH may induce gliomagenesis by similar mechanisms. J Neuropathol Exp Neurol 82(1):99–100
11. Tauziède-Espariat A, Saffroy R, Pagès M, Pallud J, Legrand L, Besnard A et al (2018) Cerebellar high-grade gliomas do not present the same

molecular alterations as supratentorial high-grade gliomas and may show histone H3 gene mutations. Clin Neuropathol 37(5):209–216
12. Pfister S, Remke M, Benner A, Mendrzyk F, Toedt G, Felsberg J et al (2009) Outcome prediction in pediatric medulloblastoma based on DNA copy-number aberrations of chromosomes 6q and 17q and the MYC and MYCN loci. J Clin Oncol Off J Am Soc Clin Oncol 27(10):1627–1636
13. Dobin A, Davis CA, Schlesinger F, Drenkow J, Zaleski C, Jha S et al (2013) STAR: ultrafast universal RNA-seq aligner. Bioinformatics 29(1):15–21
14. Chen X, Schulz-Trieglaff O, Shaw R, Barnes B, Schlesinger F, Källberg M et al (2016) Manta: rapid detection of structural variants and indels for germline and cancer sequencing applications. Bioinformatics 32(8):1220–1222
15. Banan R, Stichel D, Bleck A, Hong B, Lehmann U, Suwala A et al (2020) Infratentorial IDH-mutant astrocytoma is a distinct subtype. Acta Neuropathol (Berl) 140(4):569–581
16. Ikemura M, Shibahara J, Mukasa A, Takayanagi S, Aihara K, Saito N et al (2016) Utility of ATRX immunohistochemistry in diagnosis of adult diffuse gliomas. Histopathology 69(2):260–267
17. Lass U, Nümann A, von Eckardstein K, Kiwit J, Stockhammer F, Horaczek JA et al (2012) Clonal analysis in recurrent astrocytic, oligoastrocytic and oligodendroglial tumors implicates IDH1- mutation as common tumor initiating event. PLoS ONE 7(7):e41298
18. Landvater R, Tripathy A, Nieblas-Bedolla E, Shao L, Conway K, Al-Holou W et al (2024) Sarcomatous transformation of IDH-mutant astrocytoma matching to methylation class oligosarcoma following embolization, a case report. Acta Neuropathol Commun 12(1):196
19. Yamaguchi J, Ohka F, Seki M, Motomura K, Deguchi S, Shiba Y et al (2024) Dual phenotypes in recurrent astrocytoma, IDH-mutant; coexistence of IDH-mutant and IDH-wildtype components: a case report with genetic and epigenetic analysis. Acta Neuropathol Commun 12(1):169
20. Hinz F, Friedel D, Korshunov A, Ippen FM, Bogumil H, Banan R et al (2025) IDH-mutant astrocytomas with primitive neuronal component have a distinct methylation profile and a higher risk of leptomeningeal spread. Acta Neuropathol (Berl) 149(1):12
21. Suwala AK, Stichel D, Schrimpf D, Maas SLN, Sill M, Dohmen H et al (2021) Glioblastomas with primitive neuronal component harbor a distinct methylation and copy-number profile with inactivation of TP53, PTEN, and RB1. Acta Neuropathol (Berl) 142(1):179–189
22. Chkheidze R, Raisanen J, Gagan J, Richardson TE, Pinho MC, Raj K et al (2021) Alterations in the RB Pathway with inactivation of RB1 characterize glioblastomas with a primitive neuronal component. J Neuropathol Exp Neurol 80(12):1092–1098
23. Valcarcel-Jimenez L, Frezza C (2023) Fumarate hydratase (FH) and cancer: a paradigm of oncometabolism. Br J Cancer 129(10):1546–1557
24. Smith SC, Trpkov K, Chen YB, Mehra R, Sirohi D, Ohe C et al (2016) Tubulocystic carcinoma of the kidney with poorly differentiated foci: a frequent morphologic pattern of fumarate hydratase-deficient renal cell carcinoma. Am J Surg Pathol 40(11):1457–1472
25. Harrison WJ, Andrici J, Maclean F, Madadi-Ghahan R, Farzin M, Sioson L et al (2016) Fumarate hydratase-deficient uterine leiomyomas occur in both the syndromic and sporadic settings. Am J Surg Pathol 40(5):599–607
26. Cimino PJ, Ketchum C, Turakulov R, Singh O, Abdullaev Z, Giannini C et al (2023) Expanded analysis of high-grade astrocytoma with piloid features identifies an epigenetically and clinically distinct subtype associated with neurofibromatosis type 1. Acta Neuropathol (Berl) 145(1):71–82
27. Rudolf MA, Ferris SP (2025) High-grade astrocytoma with piloid features. Arch Pathol Lab Med. https://doi.org/10.5858/arpa.2024-0268-RA
28. Staunton J, Ajuyah P, Harris A, Mayoh C, Wong M, Rumford M et al (2024) Novel paediatric case of a spinal high-grade astrocytoma with piloid features in a patient with Noonan Syndrome. NPJ Precis Oncol 8(1):236
29. Brennan CW, Verhaak RGW, McKenna A, Campos B, Noushmehr H, Salama SR et al (2013) The somatic genomic landscape of glioblastoma. Cell 155(2):462–477

Publisher's Note